The Delineation of Fiducial Points for Non-contact Radar Seismocardiogram Signals without Concurrent ECG

Zongyang Xia, *Student Member, IEEE*, Md. Mobashir Hasan Shandhi, *Student Member, IEEE*, Yinghao Li, Omer T. Inan, *Senior Member, IEEE*, and Ying Zhang, *Senior Member, IEEE*

***Abstract*— *Objective:* Non-contact sensing of seismocardiogram (SCG) signals through a microwave Doppler radar is promising for biomedical applications. However, the delineation of fiducial points for radar SCG still relies on concurrent ECG which requires a contact sensor and limits the complete non-contact detection of SCG. *Methods:* Instead of ECG, a new reference signal, the radar displacement signal of heartbeat (RDH), was derived through the complex Fourier transform and the band pass filtering of the radar signal. The RDH signal was used to locate each cardiac cycle and mask the systolic profile, which was further used to detect an important fiducial point, aortic valve opening (AO). The beat-to-beat interval was estimated from AO-AO interval and compared with the gold standard, ECG R-to-R interval. *Results:* For the 22 subjects in the study, the evaluation of the AOs detected by RDH (AO_{RDH}) shows the average detection ratio can reach 90%, indicating a high ratio of the AO_{RDH} that are exactly the same as AO detected using the ECG R-wave (AO_{ECG}). Additionally, the left ventricular ejection time (LVET) values estimated from the ensemble averaged radar waveform through AO_{RDH} segmentation are within 2 ms of those through AO_{ECG} segmentation, for all the detected subjects. Further analysis demonstrates that the beat-to-beat intervals calculated from AO_{RDH} have an average root-mean-square-deviation (RMSD) of 53.73 ms when compared with ECG R-to-R intervals, and have an average RMSD of 23.47 ms after removing the beats in which AO cannot be identified. *Conclusions:* Radar signal RDH can be used as a reference signal to delineate fiducial points for non-contact radar SCG signals. *Significance:* This study can be applied to develop complete non-contact sensing of SCG and monitoring of vital signs, where contact-based SCG is not feasible.**

***Index Terms*— Fiducial Point, seismocardiogram (SCG), aortic valve open, non-contact, microwave, Doppler radar.**

I. Introduction

CARDIAC time intervals, such as systolic time intervals (STIs) within each cardiac cycle, are important timing features for evaluating cardiovascular health [1]–[3]. The seismocardiogram (SCG) signal, which could be measured non-invasively, records micro-scale precordial vibrations from heart movement and blood flow [4]. It can be used to derive STIs through detection of key fiducial points. These points, such as aortic valve opening (AO) and aortic valve closing (AC), can be accurately delineated from high quality SCG signals. The measured STIs can then be used to evaluate cardiac health and performance, such as exercise capacity, coronary artery disease and left ventricular muscle dysfunction [5], [6].

The conventional SCG signal is generally acquired by attaching an accelerometer to the mid-sternum [7]; while this measurement approach is non-invasive, it still requires a sensor to be attached to the skin, which may not be possible for burn patients or infants [8]–[10]. Recently, Xia et al. [11] investigated a non-contact approach based on microwave Doppler radar for SCG measurement, and demonstrated that the radar acceleration waveform (RAW, the second derivative of radar displacement signal) has a high similarity to the dorso-ventral SCG (SCG_{DV}) in both morphology and the locations of fiducial points AO and AC. Since the manual analysis used in [11] relies on the contact electrocardiogram (ECG) signal, an automatic and standalone method for delineating fiducial points from RAW, the radar SCG signal, is needed for real-time and remote monitoring of STIs.

As RAW shows high similarity to SCG_{DV}, we first explored the traditional delineation methods for SCG to delineate fiducial points from RAW. The conventional methods rely on the ECG R-wave to segment the cardiac cycles and identify the fiducial points [7], [11]. For example, the AO can be detected by searching the minimum or maximum absolute magnitude of SCG in the first 200 ms starting from the ECG R-wave [12]. The time durations between R-wave and AO, and AO and AC can represent the pre-ejection period (PEP) and left ventricular ejection time (LVET) respectively [13], [14], which are important STIs reflecting left ventricular function and having significance in heart failure monitoring [15], ischemic myocardial disease [16] and hemorrhage management [17]. However, this delineation approach requires additional ECG sensors attached to the skin surface, which is not suitable for a complete non-contact radar system.

Tadi et al. [18] developed an algorithm to detect the AO from SCG without the concurrent ECG. The algorithm combines the SCG signals in three axes to obtain the Hilbert transformed acceleration and generate the principal velocity signal. Using the local maximum of the principal velocity signal, the systolic peak or SCG AO point on the original SCG

The authors are with the School of Electrical and Computer Engineering, Georgia Institute of Technology, Atlanta, GA, 30332 USA (e-mail: zxia30@gatech.edu; mobashir.shandhi@gatech.edu; yinghaoli@gatech.edu; omer.inan@ece.gatech.edu; yzhang@gatech.edu).

signal can be located for each cardiac cycle. After removing the motion artifacts, the inter-beat intervals were calculated from the SCG AO points. They show high correlation and an average root mean square deviation (RMSD) of 37.6 ms when compared with ECG R-to-R intervals. This demonstrates a promising application of SCG in estimating the inter-beat intervals. However, the delineation algorithm of AO is susceptible to noise and requires three-axis SCG, which cannot be used for delineating the RAW signals that represent only the SCG_{DV} signals.

Khosrow-Khavar et al. [19] proposed an automatic delineation algorithm applicable to SCG_{DV} signals. Instead of using ECG, the delineation algorithm is based on an envelope signal of SCG_{DV}, the heart rate envelope (HRE), that can indicate the systolic profile of the corresponding SCG_{DV}. The delineation algorithm could identify the AO with a mean detection ratio of 32% per individual recording [19]. However, the derivation of HRE depends on the cut-off frequency, integration width and percentage of causality index, and may require adjustment for different subjects or the same subject under different conditions. Additionally, the fiducial points are unrecognizable when the signal quality of SCG_{DV} is limited.

Variational mode decomposition (VMD) approach [20] was proposed to construct the heart rate envelope, but it is for the standalone heartbeat extraction only. The moving average approach [21] and single-layer bi-directional long short-term memory (LSTM) network [22] were developed to recognize the systolic profile without concurrent ECG, which can be further applied for AO detection. However, the moving average threshold has requirements on the signal quality and the LSTM network fails to detect the systolic profiles of lower magnitude or quality, and the overall detection ratios are limited.

As discussed above, the signal quality plays an important role in the standalone delineation of fiducial points. However, compared with conventional SCG signals detected by a contact sensor, the signal quality of RAW is affected by the noise and interference in the radar transmission path. This limits the annotation performance, and in particular, the noise and interference make it difficult to accurately determine a search window for fiducial points using the methods developed for conventional SCG signals.

In this paper, we propose an approach based on a radar displacement signal of heartbeat (RDH) for automatic detection of AO from RAW without concurrent ECG. The RDH signals were derived from the complex Fourier transform of the radar displacement signals that were further band-pass filtered. The derived RDH signal was used as a reference signal to automatically and accurately narrow down search windows for standalone AO annotation, and the AOs were then detected within the search windows (AO_{RDH}). Another method using radar acceleration envelopes (RAE) was also applied to detect AOs (AO_{RAE}), based on the work of Khosrow-khavar et al. [19], and the detection ratio of AO_{RDH} was compared with that of the AO_{RAE}. Additionally, the AO and AC points were extracted from ensemble averaged waveform of the RAW signal to estimate the LVET. Finally, the inter-beat intervals calculated from the RAW AO-AO intervals were compared with the ECG R-to-R intervals to illustrate the efficacy of obtaining heart rate variability without concurrent ECG.

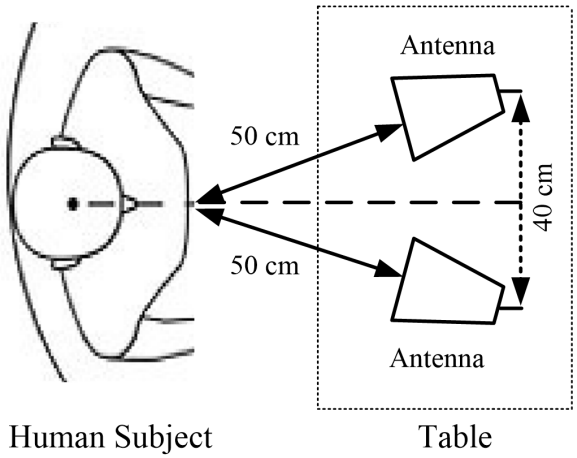

Fig. 1: Radar system setup for detecting the cardiac signals.

II. Methodology

A. Data Acquisition

The microwave Doppler radar system had the same setup as that described in [11], consisting of a microwave signal generator (Agilent N5222A), horn antennas (A-INFOLB-20180-SF), an I/Q frequency downconverter (Hittite HMC951LP4E) and a data acquisition unit (DAQ, Analog Devices AD7770). It worked at 5.8 GHz with a transmitting power of 6 dBm, and antennas were 50 cm away from the mid-sternum of a human subject as shown in Fig. 1. The I/Q radar signals were recorded from the radar system through the AD7770. The ECG was recorded using a BN-RSPEC and a MP150WSW DAQ (BioPAC Systems, Inc., Goleta, CA, USA) as a reference signal for heartbeat segmentation and fiducial point detection. The AD7770 and MP150WSW DAQs were synchronized to sample the radar and ECG signals simultaneously with the same sampling rate of 1000 samples/second.

A total of 22 individuals volunteered to participate in the experimental measurement, including 10 female adults (Age: 32.40±10.81 years, Height: 163.88±2.80 cm, and Weight: 55.75±4.61 kg) and 12 male adults (Age: 34.17±10.60 years, Height: 177.38±5.01 cm, and Weight: 77.61±7.09 kg). Before the experiments, all the participants were informed of the experimental procedures, and signed the consent forms (approved by the Georgia Tech Institutional Review Board). Each of the volunteers was asked to sit on the chair for 120 seconds for acquiring the cardiac signals in the rest state with normal breathing. Additionally, the subjects were asked to stay still to reduce motion artifacts during the measurements, such as gestures, swallow activity and other body movements.

B. Signal Processing and Reference Signal for RAW

1) Pre-processing and Linear Filtering: The radar displacement signals were obtained from the recorded I/Q radar signals through the arctangent approach [23]. Then the RAW signal was obtained by taking the second derivative of radar displacement signal, which is an acceleration signal similar to

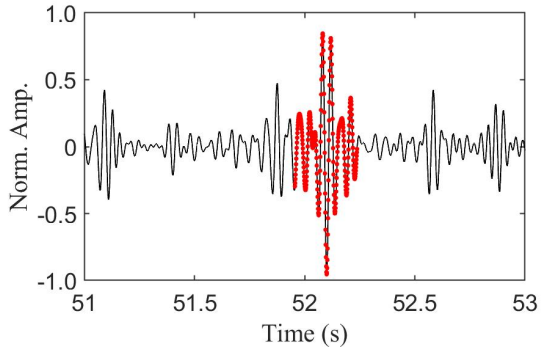

Fig. 2: Interference in the RAW signal, with interference marked with red dots.

SCG_{DV} [11]. The first and last 10 seconds were disregarded to remove the possible interferences at the beginning and end of the recording process. Thus, RAW signals of 100 seconds were analyzed for each subject.

Severe interferences due to motion artifacts such as unintentional body movement and coughs can distort the RAW signal and make it impossible to extract effective cardiac information. Typically, these interferences could result in a much higher power level than the normal cardiac signals [2]. A sliding window of length 500 ms and a threshold twice the median value of the power envelope were used to mark the interfered signals [2], as shown in Fig. 2. These marked interfered signals were discarded before further analysis.

After removing the segments corrupted with obvious motion artifacts, the ECG and RAW signals were filtered with finite impulse response (FIR) filters (Kaiser window) to remove noises with pass bands of 3-45 Hz and 18-35 Hz, respectively. The pass band of 18-35 Hz was selected for filtering RAW signal based on the previous work by Xia et al. [11]. It was demonstrated that the RAW signal in the pass band of 18-35 Hz has a good similarity to SCG_{DV} in morphology and timing features.

2) Generation of Reference Signal: A reference signal was derived to delineate the RAW signals. This reference signal was named as radar displacement signal of heartbeat (RDH), which is the displacement signal corresponding to the heartbeat that is much smaller than and is superimposed on the respiration signal as shown in Fig. 3 (a). To extract the RDH signal, a complex Fourier transform (CFT) was first applied to the recorded radar displacement signals to eliminate the harmonics and signal distortion in the spectrum [24]. As shown in Fig. 3 (b), the spectrum can clearly show the heartbeat component at 1.285 Hz without the surrounding interferences. By searching for the highest peak within the frequency band 0.8 Hz-2.5 Hz where the heartbeat frequency generally locates [25], the heartbeat frequency (f_{hb}) could be identified. Then, a FIR filter with 0.2-Hz pass band centering on the heartbeat frequency $[f_{hb} - 0.1, f_{hb} + 0.1]$ was applied to the radar displacement signals to extract the RDH signal. This indicates the maximum allowable change of heart rate for the duration of the radar signal that uses a single RDH reference signal is 6 beats per minute. For general applications, wherein the heart

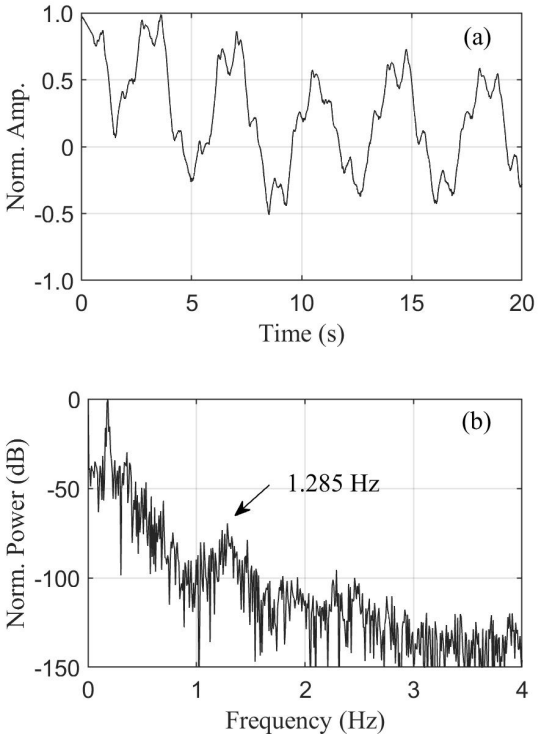

Fig. 3: Radar displacement signal in (a) the time domain, and (b) the frequency domain.

rate may vary more than 6 beats per minute over time, the radar recording may be segmented into multiple sections so that the variation of heart rate is within 6 beats per minute within each section. Then a RDH signal could be extracted from each of the multiple sections using the proposed approach.

C. Window Selection for Masking Systolic Profile and Searching Fiducial Point AO

For determining the AO location in SCG, the ECG R-wave is typically used as the reference, and the peak of SCG with the minimum or maximum absolute magnitude within a 200-ms fixed window is considered as the AO point [12], [26]. This method was applied to RAW, the radar SCG signal, to obtain the accurate AO locations for evaluating the proposed method in this paper, which was denoted as AO_{ECG}.

In the proposed method that uses the RDH signal as a reference signal, two windows were determined to mask the systolic profile and search the AO point, respectively. The RAW of 16 subjects were analyzed to obtain the two windows. Based on our observation, the peaks of RDH (PRDH) might be at either side of the ECG R-wave. The locations of PRDH relative to the ECG R-wave should be evaluated to correctly build a 300-ms time window for locating the systolic profile. The relative locations of PRDH with respect to the ECG R-wave were analyzed for all heartbeats of each subject. For the heartbeats with PRDH before ECG R-wave, the 300-ms window starting from or before PRDH could mask the systolic profile. For heartbeats with PRDH after ECG R-wave, the window should be adjusted, and the analysis of the interval between them could determine the 95% confidence

interval and a number *offset1*, which determines a 300-ms time window [*PRDH-offset1, PRDH-offset1+300*] that can mask the major portion of the systolic profile in general cases. After masking the systolic profile in RAW, the envelope of the profile (ENV_{RDH}) was derived through a third order integration of the masked RAW, and the peak of ENV_{RDH} ($PENV_{RDH}$) should be very close to the AO point [27]. The $PENV_{RDH}$ was found around the location of the corresponding AO_{ECG} which is considered as the true location of AO. The relative location of $PENV_{RDH}$ with respect to AO_{ECG} was evaluated to determine a general search window for AO. Similar with the determination of 300-ms window, the intervals between $PENV_{RDH}$ and AO_{ECG} for heartbeats with $PENV_{RDH}$ after AO_{ECG} were analyzed to obtain the 95% confidence interval, which could determine an *offset2*. A 200-ms time window [$PENV_{RDH}$-*offset2, *$PENV_{RDH}$-*offset2+200*] can be built to search for the AO_{RDH}. The peak of RAW with the minimum or maximum absolute magnitude in this 200-ms fixed window is considered as the AO, denoted as AO_{RDH}. The process for identifying AO_{RDH} is shown in Algorithm 1. The locating, integrating and searching processes contribute to a computational complexity of $O(n)$ for the algorithm, where n represents the length of the radar signal.

Algorithm 1 Identify the fiducial point AO_{RDH}

1: Locate the peaks of RDH (*PRDH*)
2: Use *PRDH* to build 300-ms windows, [*PRDH-offset1, PRDH-offset1+300*]
3: Within the 300-ms window, mask the systolic profile
4: Integrate the masked profile to get its envelope ENV_{RDH}
5: Locate the peaks of ENV_{RDH} ($PENV_{RDH}$)
6: Use $PENV_{RDH}$ to build 200-ms windows, [$PENV_{RDH}$-*offset2, *$PENV_{RDH}$-*offset2+200*]
7: Within the 200-ms window, search for the minimum or maximum absolute and obtain AO_{RDH}

As mentioned before, another method using RAE was applied to detect AO from radar signal based on the work for contact SCG waveform proposed by Khosrow-khavar et al. [19]. In this approach, the peaks of RAE (PRAE) are at least 50 ms before the ECG R-wave, and therefore a fixed window of 300 ms with respect to PRAE [*PRAE, PRAE+300*] was chosen to mask the systolic profile. Then the envelope of systolic profile (ENV_{RAE}) and its peak ($PENV_{RAE}$) were derived so that the AO point can be determined as the peak with maximum or minimum absolute magnitude within a search window W_{SYS} proposed in [19]. The AO location determined using this method was denoted as AO_{RAE}.

D. Ensemble Averaged Waveform and LVET

Compared with AO, the automatic delineation of AC is more challenging due to the variations in amplitude and timing of the AC peaks in each heart beat cycle for the conventional SCG [4]. The signal quality of RAW including the amplitude and timing features is affected more by interference and noise when compared with SCG acquired from the contact sensor approach. Thus, the AC points were manually extracted from RAW, which is the first encountered maximum for the diastolic profile [28]. The AC point represents the start of diastole when the pressure inside the ventricle has dropped causing the aortic valve to close abruptly.

For each subject, the 100-second RAW signal was first segmented into heartbeats using four reference points: ECG R-wave, AO_{ECG}, AO_{RAE} and AO_{RDH} separately. The performance of adopting these different reference points were compared afterwards in Section III-D. All the heartbeats were averaged with ensemble averaging techniques to reduce uncorrelated noise [29]. Then, four ensemble averaged RAW heartbeats were obtained for each subject.

After averaging, the AC point on each ensemble averaged waveform was manually marked. For each subject, the AC_R, AC_{ECG}, AC_{RAE} and AC_{RDH} were obtained, and they represent the ACs identified in the ensemble averaged waveforms segmented by ECG R-wave, AO_{ECG}, AO_{RAE} and AO_{RDH}, respectively. LVET was then determined by calculating the AO-AC interval. The LVETs derived from the ensemble averaged waveforms obtained by using ECG R-wave, AO_{ECG}, AO_{RAE} and AO_{RDH} as reference points were denoted as $LVET_R$, $LVET_{ECG}$, $LVET_{RAE}$ and $LVET_{RDH}$, respectively.

E. Interbeat Interval from AO

Tadi et al. has shown that AO-AO interval of SCG can be used to obtain beat to beat interval (BBI) with a high accuracy when compared with corresponding ECG R-to-R interval [18]. Apart from estimating STIs, studies were also conducted to explore the efficacy of using the AO points delineated from the RAW signal to estimate BBI. The BBIs calculated using the AO_{ECG}, AO_{RAE} and AO_{RDH} were denoted as BBI_{ECG}, BBI_{RAE} and BBI_{RDH}, respectively. Those BBI values were also compared with the gold standard BBI that is the ECE R-to-R interval and was denoted as BBI_R.

III. Experimental Evaluation

A. The Performance of the Reference Signal RDH

A visual comparison of RAE and RDH with corresponding ECG and RAW signals is given in Fig. 4. The RDH signal was compared with the ECG and RAE signals to evaluate its performance. Fig. 4 (a) shows an example of good-quality RAW signal whereas Fig. 4 (b) gives an example of poor-quality RAW signal. In both cases, the RAE and RDH signals show the same number of cardiac cycles as that of ECG, and each cycle has a major peak that could potentially be used as a reference point similar to the ECG R-wave. The RDH signal has peak locations different from the RAE signal, and contains less tiny fluctuations.

It is obvious that the cardiac cycles cannot be accurately determined from only a RAE signal derived from the relatively low-quality radar signal, as shown in Fig. 4 (b). The time interval between adjacent peaks is affected due to the noise and the interferences, and the effectiveness of RAE is severely degraded. This was also demonstrated in [19]. For example, in Fig. 4 (b), the fifth peak in RAE is less than 400 ms from its previous peak and should be disregarded, and thus this cardiac cycle could not be identified by RAE. In contrast to the RAE

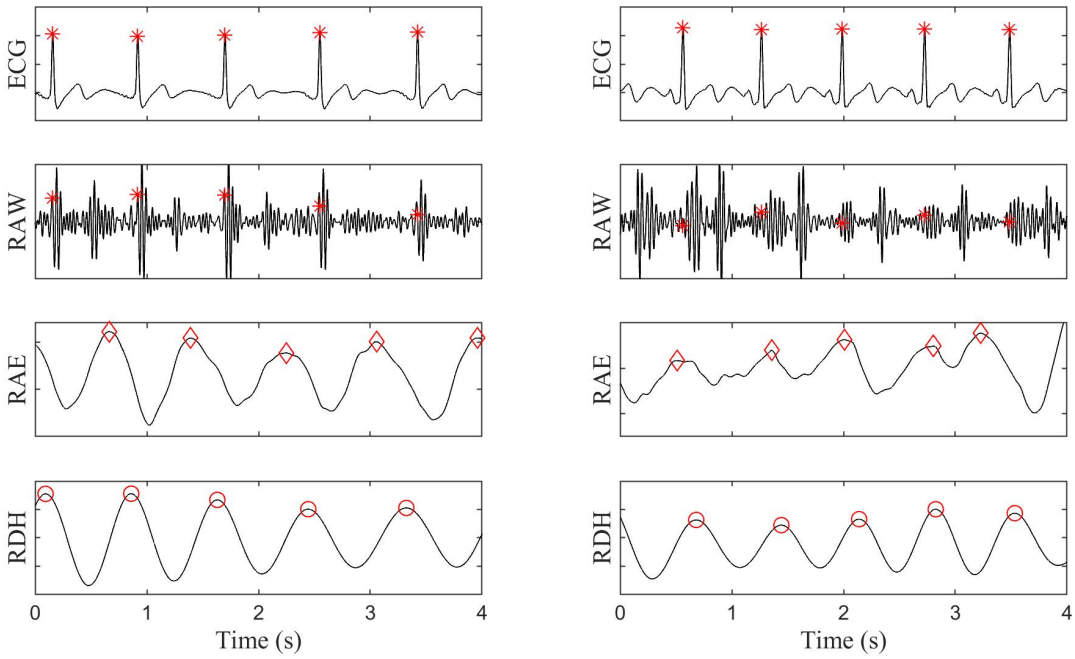

(a) A high-quality RAW

(b) A low-quality RAW

Fig. 4: ECG, RAE and RDH for the RAW with red stars representing ECG R-peaks, red diamonds indicating the peaks of RAE, and red circles showing the peaks of RDH.

signal, the RDH signal in Fig. 4 (b) is showing to be less affected by the noise and can still indicate the cardiac cycles correctly. Since the center frequency of the band pass filter, described in Section II-B.2, is an estimation of the averaged heartbeat, the band pass filtering step reduces the influence of sudden interference.

To further evaluate the performance of RDH and RAE in representing the cardiac cycle quantitatively, the number of detected cardiac cycles using the ECG, RAE and RDH signals was compared for each of the 22 subjects. ECG is the gold standard for identifying cardiac cycles in healthy people without arrhythmias, and number of cardiac cycles in ECG is denoted as N. The ratio between the number of detected cardiac cycles in RAE and N, $\mathrm{r_{RAE}}$, and the ratio between that in RDH and N, $\mathrm{r_{RDH}}$, are shown in Fig. 5.

As shown in Fig. 5, the RDH signal provides a high average detection ratio of cardiac cycles, 0.995. Among the 22 subjects, it detects the same number of cardiac cycles as that from ECG for 16 subjects, and the detection ratio is over 0.96 for the other 6 subjects. In comparison, the RAE signal achieves an average detection ratio of 0.883, lower than that of RDH, and provides the same number of cardiac cycles as that from ECG for only 2 subjects. Thus, the RDH signal could represent the number of cardiac cycles accurately, and would be promising to locate the systolic profile and the fiducial point.

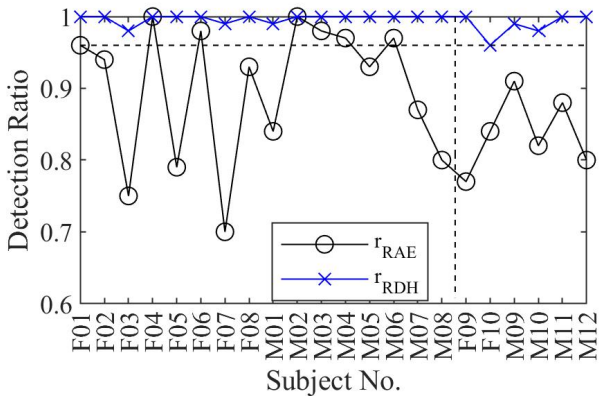

Fig. 5: The detection ratios of cardiac cycles of RAE and RDH. Here, F and M stand for female and male subjects, respectively. For example, F1 represents the female subject 1.

B. The Determination of the Time Window

For the heartbeats with PRDH before the ECG R-wave, the time window [*PRDH-offset1, PRDH-offset1+300*] could mask the systolic profile. However, it should be adjusted to guarantee the masking of systolic profile for the heartbeats with PRDH after the ECG R-wave. The intervals between PRDH and ECG R-wave for 16 subjects were analyzed to determine the *offset1* value, and the other 6 subjects were used to evaluate the performance of *offset1* in the fiducial point annotation. Fig. 6 summarizes the time interval for heartbeats in which PRDH is on the right of corresponding ECG R-wave.

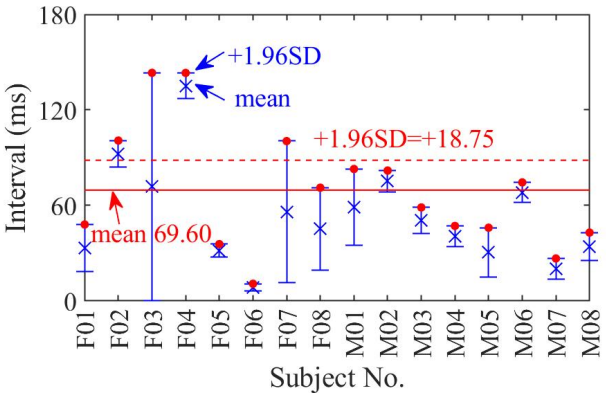

Fig. 6: The time interval between PRDH and ECG R-wave for heartbeats with PRDH after ECG R-wave.

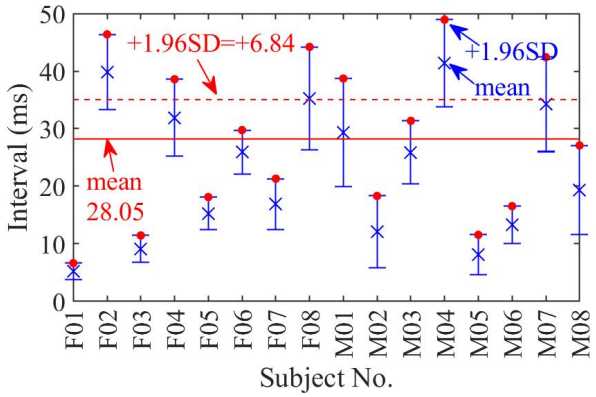

Fig. 7: The time interval between $PENV_{RDH}$ and AO_{ECG} for heartbeats with $PENV_{RDH}$ after AO_{ECG}.

Based on the statistical analysis of confidence interval [30], [31], the 95% confidence interval for each subject was calculated. Using the upper confidence limit marked in red dot for each subject, the 95% confidence interval for the 16 subjects could determine the *offset1* to be 88.35 ms, and a 300-ms time window [*PRDH-88.35, PRDH+211.65*] was selected for masking the systolic profile. For the heartbeats with PRDH after the ECG R-wave, Fig. 6 shows that 14 out of 16 subjects have mean values within 88.35 ms, and thus the window could mask the systolic profile in general cases.

After determining the time window for masking the systolic profile, $PENV_{RDH}$ was obtained from the envelope of the masked systolic profile. The intervals between $PENV_{RDH}$ and AO_{ECG} were evaluated to determine the time window [$PENV_{RDH}$*-offset2,* $PENV_{RDH}$*-offset2+200*]. Similar with the determination of 300-ms window, Fig. 7 shows the analysis of time interval between $PENV_{RDH}$ and AO_{ECG} points for the heartbeats with $PENV_{RDH}$ on the right of AO_{ECG} points.

As shown in Fig. 7, the 95% confidence interval for each of 16 subjects was calculated, and the upper confidence limit marked in red dot determined the 95% confidence interval for 16 subjects. Then the *offset2* was determined to be 34.89 ms, and a 200-ms time window of [$PENV_{RDH}$*-34.89,* $PENV_{RDH}$*+165.11*] was selected to search for AO_{RDH}.

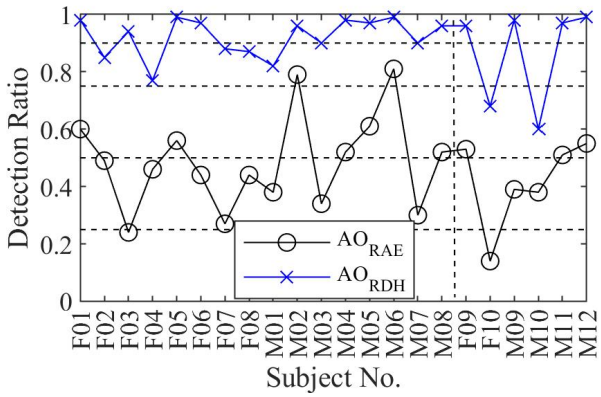

Fig. 8: The detection ratios of AO_{RAE} and AO_{RDH}.

C. Evaluation of the Fiducial Point AO

The detection ratios of AO_{RAE} and AO_{RDH} for each subject were assessed to demonstrate the detection accuracy. Here, the detection ratio indicates the percentage of number of AO_{RAE} or AO_{RDH} that are at the same locations as that of the corresponding AO_{ECG}. The results for the 16 subjects are presented in Fig. 8, and those of the last 6 subjects in Fig.8 are also demonstrated to exhibit the detection performance.

For the first 16 subjects, the detection ratios of AO_{RDH} are all over 75%, in which 11 of them are over 90%. The results of AO_{RAE} exhibit that for only 2 subjects the detection ratios are over 75%, for 5 subjects the rations are between 50% and 75%, and for 9 subjects the detection ratios are between 25% and 50%.

For the other 6 subjects, the AO_{RDH} has detection ratios over 90% for 4 subjects and the ratios are between 50% and 75% for 2 subjects. For AO_{RAE}, the detection ratios are between 50% and 75% for 3 subjects, the ratios are between 25% and 50% for 2 subjects, and for the subject F10 the detection ratio is below 25%.

Based on the results in Fig. 8, AO_{RDH} achieves an overall average detection ratio of 90%. For the case of AO_{RAE}, the average detection ratio is 47%. The results demonstrate that AO_{RDH} could achieve a good representation of AO_{ECG}, and improve the average detection ratio by 43% when compared with AO_{RAE}.

The superior performance of AO_{RDH} compared with AO_{RAE} is due to the high quality of the RDH signal that leads to a higher detection ratio of cardiac cycles and better determined windows, as demonstrated in Sections III-A and III-B. This in turn helps to obtain more accurate systolic profiles using RDH, which is further demonstrated visually in Fig. 9. In Fig. 9 (a), a high-quality RAW signal is presented with the corresponding AO_{ECG}, AO_{RAE} and AO_{RDH} marked. In addition, the ECG R-wave location, ENV_{RAE} and ENV_{RDH} were also marked and displayed. Here, a high-quality RAW signal indicates that it has a cross correlation coefficient over 0.9 with the concurrent dorso-ventral SCG detected by an accelerometer. The figure shows that each ECG R-wave locates before the corresponding AO, while the peaks of ENV_{RAE} and ENV_{RDH} are very close to the corresponding AO point. The AO localization methods

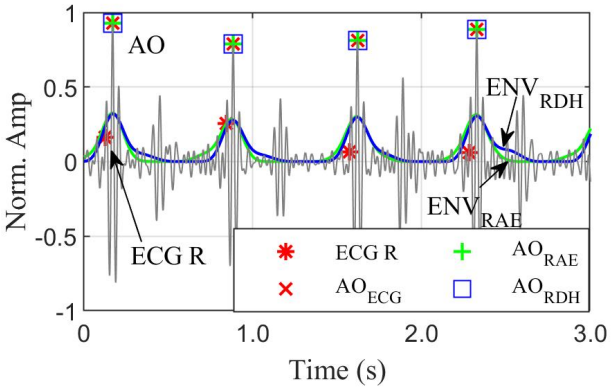

(a) A high-quality RAW

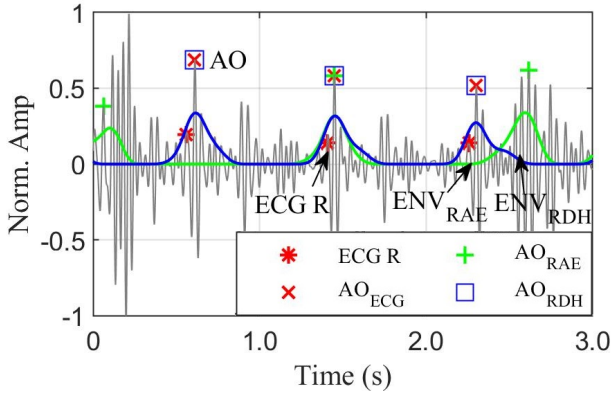

(b) A low-quality RAW

Fig. 9: Detection of fiducial point AO from radar signals using ECG, RAE and RDH.

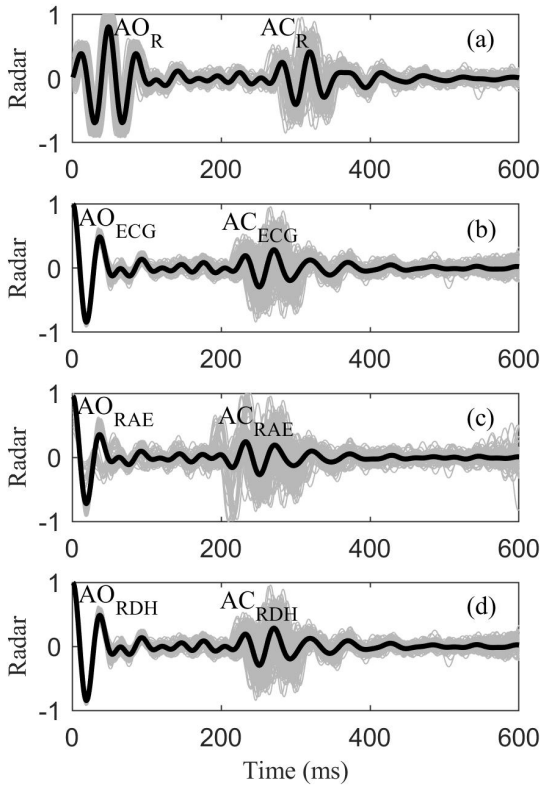

Fig. 10: The averaged RAW waveform starting from (a) ECG R-wave, (b) AO_{ECG}, (c) AO_{RAE} and (d) AO_{RDH}.

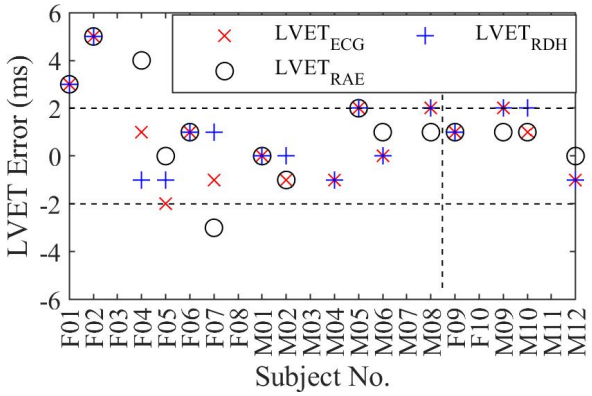

Fig. 11: The errors of the LVETs derived from the ensemble averaged RAW with $LVET_R$ as the reference.

based on the peaks of ENV_{RAE} and ENV_{RDH}, as discussed in Section II-C, can accurately locate AO_{RAE} and AO_{RDH}, respectively, which are at the same locations as that of AO_{ECG}. However, when the signal quality of RAW decreases, as shown in Fig. 9 (b), the RAE approach fails to detect some AO points while the RDH approach could still reliably identify all AO points, which demonstrates the robustness of the RDH approach to the noise.

D. Evaluation of the Ensemble Averaged Waveform and LVET

The ensemble averaged waveform for one subject is shown in Fig. 10. Fig. 10 (a) is the ensemble average of the beats segmented using the ECG R-wave. The fiducial points AO_R and AC_R are clearly observed, and the ensemble average exhibits high signal quality. The waveforms in Figs. 10 (b), (c) and (d) correspond to the ensemble average of beats segmented using AO_{ECG}, AO_{RAE} and AO_{RDH}, respectively.

The morphology of Fig. 10 (b) is very similar to that of Fig. 10 (a), except that the starting point is AO_{ECG} instead of ECG R-wave. After removing the part before AO_R of Fig. 10 (a) and the corresponding number of points at the end of Fig. 10 (b), the averaged waveforms in Figs. 10 (a) and (b) have a cross correlation coefficient of 0.97. The high similarity of the averaged waveforms indicates that the beat segmentation with AO could also be effectively used for obtaining the ensemble averaged waveform.

The averaged waveform in Fig. 10 (d) has a cross correlation coefficient of 0.99 to that in Fig. 10 (b), which is higher than the coefficient of 0.95 between the waveforms in Figs. 10 (b) and (c). Thus, compared with Fig. 10 (c), the averaged waveform in Fig. 10 (d) has higher similarity to Fig. 10 (b) in morphology, especially the diastolic profile. This is because the AO_{RDH} has a higher detection ratio, and thus reduces the number of beats that are not starting from the correct

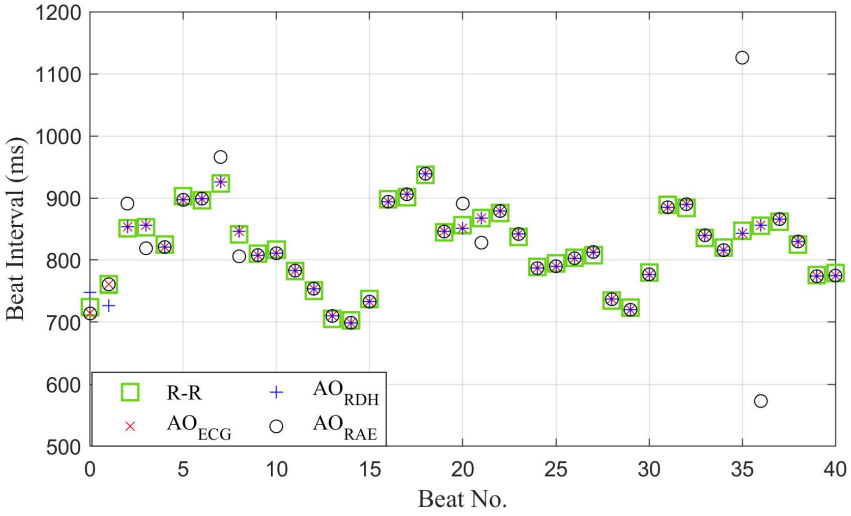

Fig. 12: Beat-to-beat intervals calculated from AO for one subject.

AO locations. The beats starting from inaccurate AO points degrade the morphology of the ensemble averaged waveform, as observed in Fig. 10 (b) at around 200 ms.

To evaluate the performance of using different reference signals for estimating LVETs, LVETs for each subject were calculated from AOs and ACs marked on the corresponding ensemble averaged waveforms. For the LVETs obtained using three reference points (AO_{ECG}, AO_{RAE} and AO_{RDH}), the comparisons with $LVET_R$ are given in Fig. 11.

For subjects F03, F10 and M07, ACs could not be identified from the ensemble averaged RAW waveforms due to the limited quality of RAW, and thus the corresponding LVETs are not available. For the other 19 subjects, the $LVET_R$ are detected. Compared with the $LVET_R$, the $LVET_{ECG}$ is within 2 ms of $LVET_R$ for 14 subjects and the errors are between 2 ms and 5 ms for 2 subjects. For the other 3 subjects, ACs are undetectable on the quality-limited ensemble averaged waveform starting from AO_{ECG}, and thus $LVET_{ECG}$ are not available. This indicates that the beat segmentation with AO can be used to estimate LVET with limited errors.

The $LVET_{RDH}$ has almost the same results as that of the $LVET_{ECG}$. For each detected $LVET_{ECG}$, the corresponding $LVET_{RDH}$ is within 2 ms. The $LVET_{RAE}$ could also achieve good performances, but F04 and F07 have deviations over 2 ms and the method does not provide a $LVET_{RAE}$ value for M04. These results demonstrate that $LVET_{RDH}$ could perform as well as $LVET_{ECG}$, and has better performance than $LVET_{RAE}$.

E. Evaluation of Interbeat Interval from AO

BBIs calculated from AO-AO intervals are compared with the gold standard BBI_R for one subject with a 30-second plot shown in Fig. 12. The variation of the BBI_R and BBI_{ECG} with time demonstrates the respiratory trends congruent with physiological mechanisms of respiratory sinus arrhythmia [32]. The BBI_{RAE} and BBI_{RDH} also indicate the similar results and follow the respiratory trends. In Fig. 12, the BBI_{RDH} are the same as the BBI_R except the two points at the beginning of

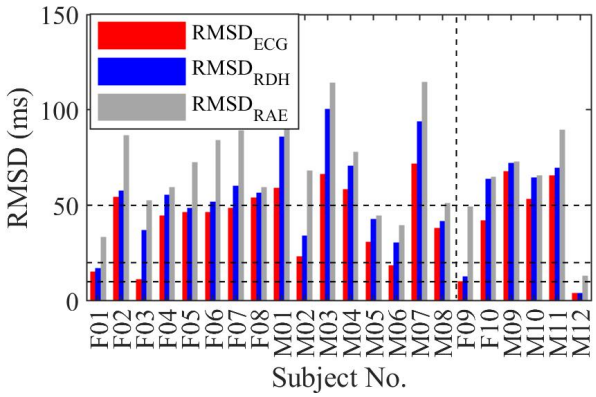

Fig. 13: The RMSDs of BBI_{ECG}, BBI_{RAE} and BBI_{RDH} using BBI_R as reference.

the plot, while the BBI_{RAE} has relatively large errors at 7 points. This is also exhibited in their RMSDs from the BBI_R, which are 6.55 ms and 64.52 ms for BBI_{RDH} and BBI_{RAE}, respectively.

To further demonstrate the accuracy of BBI_{ECG}, BBI_{RAE} and BBI_{RDH}, they are compared with the gold standard BBI_R for all the subjects. The corresponding RMSDs are calculated and denoted as $RMSD_{ECG}$, $RMSD_{RAE}$ and $RMSD_{RDH}$, respectively, with the results shown in Fig. 13.

The BBI_{ECG} is first compared with the BBI_R to demonstrate the accuracy of BBI_{ECG} in representing the gold standard BBI_R. A large variation of the $RMSD_{ECG}$ is observed for different subjects in Fig. 13. The $RMSD_{ECG}$ for 5 subjects are within 20 ms, but are over 50 ms for 9 subjects. The average $RMSD_{ECG}$ for all the subjects is 42.0 ms, which is about 5 ms larger than the results of SCG stated in [18]. The relatively large deviation is due to the additional interference in the RAW, which results in an inaccurate annotation of AO and thus introduces difference between the AO-AO and the R-R intervals.

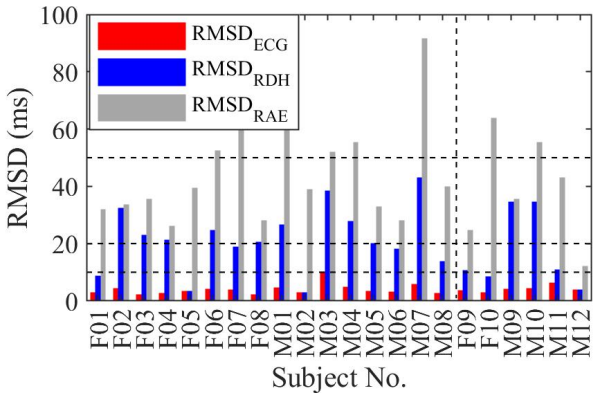

Fig. 14: The RMSDs of BBI_{ECG}, BBI_{RAE} and BBI_{RDH} after removing large deviations, with BBI_R as reference.

The averages of $RMSD_{RAE}$ and $RMSD_{RDH}$ are 69.68 ms and 53.73 ms, respectively. Compared with $RMSD_{RAE}$, the $RMSD_{RDH}$ exhibits lower deviations for all the subjects, including the 16 subjects for window selection and the other 6 subjects. This indicates that the deviations of BBI_{RDH} from BBI_R are less than that of BBI_{RAE}, and BBI_{RDH} could achieve a better representation of BBI_R.

The deviation of BBI_{ECG}, BBI_{RAE} and BBI_{RDH} from BBI_R might be due to wrong annotation of AO for poor-quality RAW, especially when the RAW signal was interfered by small interference that makes it difficult to correctly locate AO. After marking the BBI_{ECG} that has deviations over 20 ms from the corresponding BBI_R, the locations of wrong annotations can be found. To evaluate the performance of BBI_{RDH} with less interference, BBI_{ECG}, BBI_{RAE} and BBI_{RDH} at these locations are removed, which leads to the improved $RMSD_{ECG}$, $RMSD_{RAE}$ and $RMSD_{RDH}$ as shown in Fig. 14.

After removing the large deviations, $RMSD_{ECG}$ are decreased to below 10 ms for all the subjects, and the average is 3.82 ms. Compared with the corresponding RMSDs in Fig. 13, $RMSD_{RAE}$ and $RMSD_{RDH}$ in Fig. 14 are also decreased. The averages of $RMSD_{RAE}$ and $RMSD_{RDH}$ are 43.92 ms and 23.47 ms, respectively, which implies a much better performance for a high quality RAW signal.

IV. Conclusion

In this paper, an approach for detecting the AO from RAW without the concurrent ECG is presented to enable fully non-contact detection and analysis of SCG. The approach is based on a RDH signal that is derived from the radar displacement signal. The peaks of the RDH signal are used as reference points to accurately locate the systolic profiles of RAW with a fixed time window. Then the peaks of the envelope of the located systolic profiles are used as reference points for searching the AO_{RDH}. The results show that the AO_{RDH} have detection ratios over 75% for 20 out of 22 subjects, achieving a high estimation of AO points. The $LVET_{RDH}$ obtained from the ensemble averaged RAW is within 2 ms of the $LVET_{ECG}$. Additional analysis of the BBI reveals that the RDH-based approach could provide a non-contact detection of the BBI with an average RMSD of 53.73 ms, and the RMSD could be reduced to 23.47 ms after removing the large deviations or the heartbeats with relatively high interferences.

Since the RDH-based approach can detect the AO with reasonable accuracy, this paves the way towards the complete non-contact measurement and analysis of SCG and enables remote sensing of BBI using the radar system. However, more robust method may need to be developed for searching AO within the built search window, especially for signals containing noise and interference. In addition, ACs from RAW are manually delineated, which limits the automatic detection of LVET in each heartbeat cycle, and the estimation of beat-to-beat intervals from the RAW signal is limited when compared with the ECG R-to-R interval. In future work, we will improve the robustness of the detection, use concurrent conventional SCG to evaluate the accuracy of information extracted from RAW, and further investigate fiducial point detection under external perturbation such as exercise, which will promote the applications of the non-contact system in cardiovascular monitoring applications, such as hemorrhage management, cardiac computed tomographic gating [33], and monitoring patients with heart failure [34].

References

[1] D. M. Salerno and J. Zanetti, "Seismocardiography for monitoring changes in left ventricular function during ischemia," *Chest*, vol. 100, no. 4, pp. 991–993, 1991.

[2] M. J. Tadi, T. Koivisto, M. Pänkäälä, A. Paasio, T. Knuutila, M. Teräs, and P. Hänninen, "A new algorithm for segmentation of cardiac quiescent phases and cardiac time intervals using seismocardiography," in *Sixth International Conference on Graphic and Image Processing (ICGIP 2014)*, vol. 9443. International Society for Optics and Photonics, 2015, p. 94432K.

[3] J. M. Zanetti and K. Tavakolian, "Seismocardiography: Past, present and future," in *2013 35th annual international conference of the IEEE engineering in medicine and biology society (EMBC)*. IEEE, 2013, pp. 7004–7007.

[4] G. Shafiq, S. Tatinati, W. T. Ang, and K. C. Veluvolu, "Automatic identification of systolic time intervals in seismocardiogram," *Scientific reports*, vol. 6, p. 37524, 2016.

[5] P. Geleris, C. Raidis, M. Papadimitriou, H. Boudoulas, and P. Metaxas, "Effect of hemodialysis on left ventricular performance." *Journal of medicine*, vol. 14, no. 3, pp. 211–222, 1983.

[6] K. Tavakolian, "Systolic time intervals and new measurement methods," *Cardiovascular engineering and technology*, vol. 7, no. 2, pp. 118–125, 2016.

[7] O. T. Inan, P.-F. Migeotte, K.-S. Park, M. Etemadi, K. Tavakolian, R. Casanella, J. Zanetti, J. Tank, I. Funtova, G. K. Prisk *et al.*, "Ballistocardiography and seismocardiography: A review of recent advances," *IEEE journal of biomedical and health informatics*, vol. 19, no. 4, pp. 1414–1427, 2015.

[8] C. Li, Z. Peng, T.-Y. Huang, T. Fan, F.-K. Wang, T.-S. Horng, J.-M. Muñoz-Ferreras, R. Gómez-García, L. Ran, and J. Lin, "A review on recent progress of portable short-range noncontact microwave radar systems," *IEEE Transactions on Microwave Theory and Techniques*, vol. 65, no. 5, pp. 1692–1706, 2017.

[9] C. Li, J. Cummings, J. Lam, E. Graves, and W. Wu, "Radar remote monitoring of vital signs," *IEEE Microwave Magazine*, vol. 10, no. 1, pp. 47–56, 2009.

[10] Z. Xia and Y. Zhang, "Dual-carrier noncontact vital sign detection with a noise suppression scheme based on phase-locked loop," *IEEE Transactions on Microwave Theory and Techniques*, vol. 64, no. 11, pp. 4003–4011, 2016.

[11] Z. Xia, M. M. H. Shandhi, O. T. Inan, and Y. Zhang, "Non-contact sensing of seismocardiogram signals using microwave doppler radar," *IEEE Sensors Journal*, vol. 18, no. 14, pp. 5956–5964, 2018.

[12] H. Ashouri and O. T. Inan, "Automatic detection of seismocardiogram sensor misplacement for robust pre-ejection period estimation in unsupervised settings," *IEEE Sensors Journal*, vol. 17, no. 12, pp. 3805–3813, 2017.

[13] N. Z. Gurel, H. Jung, S. Hersek, and O. T. Inan, "Fusing near-infrared spectroscopy with wearable hemodynamic measurements improves classification of mental stress," *IEEE Sensors Journal*, 2018.

[14] M. Di Rienzo, E. Vaini, P. Castiglioni, P. Meriggi, and F. Rizzo, "Beat-to-beat estimation of lvet and qs2 indices of cardiac mechanics from wearable seismocardiography in ambulant subjects," in *2013 35th Annual International Conference of the IEEE Engineering in Medicine and Biology Society (EMBC)*. IEEE, 2013, pp. 7017–7020.

[15] R. Lewis, S. Rittogers, W. Froester, and H. Boudoulas, "A critical review of the systolic time intervals," *Circulation*, vol. 56, no. 2, pp. 146–158, 1977.

[16] D. M. Salerno and J. Zanetti, "Seismocardiography for monitoring changes in left ventricular function during ischemia," *Chest*, vol. 100, no. 4, pp. 991 – 993, 1991. [Online]. Available: http://www.sciencedirect.com/science/article/pii/S0012369216324904

[17] K. Tavakolian, G. A. Dumont, G. Houlton, and A. P. Blaber, "Precordial vibrations provide noninvasive detection of early-stage hemorrhage." *Shock*, vol. 41, no. 2, pp. 91–96, 2014.

[18] M. J. Tadi, E. Lehtonen, T. Hurnanen, J. Koskinen, J. Eriksson, M. Pänkäälä, M. Teräs, and T. Koivisto, "A real-time approach for heart rate monitoring using a hilbert transform in seismocardiograms," *Physiological measurement*, vol. 37, no. 11, p. 1885, 2016.

[19] F. Khosrow-Khavar, K. Tavakolian, A. Blaber, and C. Menon, "Automatic and robust delineation of the fiducial points of the seismocardiogram signal for noninvasive estimation of cardiac time intervals," *IEEE Transactions on Biomedical Engineering*, vol. 64, no. 8, pp. 1701–1710, 2016.

[20] T. Choudhary, L. N. Sharma, and M. K. Bhuyan, "Standalone heartbeat extraction in scg signal using variational mode decomposition," in *2018 International Conference on Wireless Communications, Signal Processing and Networking (WiSPNET)*, 2018, pp. 1–4.

[21] L. Luu and A. Dinh, "Using moving average method to recognize systole and diastole on seismocardiogram without ecg signal," in *2018 40th Annual International Conference of the IEEE Engineering in Medicine and Biology Society (EMBC)*, 2018, pp. 3796–3799.

[22] Y. Li, Z. Xia, and Y. Zhang, "Standalone systolic profile detection of non-contact scg signal with lstm network," *IEEE Sensors Journal*, vol. 20, no. 6, pp. 3123–3131, 2020.

[23] B.-K. Park, O. Boric-Lubecke, and V. M. Lubecke, "Arctangent demodulation with dc offset compensation in quadrature doppler radar receiver systems," *IEEE transactions on Microwave theory and techniques*, vol. 55, no. 5, pp. 1073–1079, 2007.

[24] C. Li and J. Lin, "Complex signal demodulation and random body movement cancellation techniques for non-contact vital sign detection," in *2008 IEEE MTT-S International Microwave Symposium Digest*. IEEE, 2008, pp. 567–570.

[25] S. Ivashov, V. Razevig, A. Sheyko, and I. Vasilyev, "Detection of human breathing and heartbeat by remote radar," in *Progress in Electromagnetic Research Symposium*, vol. 2004, 2004.

[26] A. Q. Javaid, H. Ashouri, A. Dorier, M. Etemadi, J. A. Heller, S. Roy, and O. T. Inan, "Quantifying and reducing motion artifacts in wearable seismocardiogram measurements during walking to assess left ventricular health," *IEEE Transactions on Biomedical Engineering*, vol. 64, no. 6, pp. 1277–1286, 2017.

[27] F. Khosrow-Khavar, K. Tavakolian, and C. Menon, "Moving toward automatic and standalone delineation of seismocardiogram signal," in *2015 37th Annual International Conference of the IEEE Engineering in Medicine and Biology Society (EMBC)*. IEEE, 2015, pp. 7163–7166.

[28] F. Khosrow-Khavar, K. Tavakolian, A. P. Blaber, J. M. Zanetti, R. Fazel-Rezai, and C. Menon, "Automatic annotation of seismocardiogram with high-frequency precordial accelerations," *IEEE journal of biomedical and health informatics*, vol. 19, no. 4, pp. 1428–1434, 2015.

[29] G. Shafiq, S. Tatinati, and K. C. Veluvolu, "Automatic annotation of peaks in seismocardiogram for systolic time intervals," in *2016 38th Annual International Conference of the IEEE Engineering in Medicine and Biology Society (EMBC)*. IEEE, 2016, pp. 2672–2675.

[30] S. Nakagawa and I. C. Cuthill, "Effect size, confidence interval and statistical significance: a practical guide for biologists," *Biological reviews*, vol. 82, no. 4, pp. 591–605, 2007.

[31] M. J. Gardner and D. G. Altman, "Confidence intervals rather than p values: estimation rather than hypothesis testing." *Br Med J (Clin Res Ed)*, vol. 292, no. 6522, pp. 746–750, 1986.

[32] K. Pandia, O. T. Inan, G. T. Kovacs, and L. Giovangrandi, "Extracting respiratory information from seismocardiogram signals acquired on the chest using a miniature accelerometer," *Physiological measurement*, vol. 33, no. 10, p. 1643, 2012.

[33] J. Yao, S. Tridandapani, C. A. Wick, and P. T. Bhatti, "Seismocardiography-based cardiac computed tomography gating using patient-specific template identification and detection," *IEEE journal of translational engineering in health and medicine*, vol. 5, pp. 1–14, 2017.

[34] O. T. Inan, M. Baran Pouyan, A. Q. Javaid, S. Dowling, M. Etemadi, A. Dorier, J. A. Heller, A. O. Bicen, S. Roy, T. De Marco *et al.*, "Novel wearable seismocardiography and machine learning algorithms can assess clinical status of heart failure patients," *Circulation: Heart Failure*, vol. 11, no. 1, p. e004313, 2018.

Zongyang Xia (S'17) received the B.S. and M.S. degree in Electrical Engineering from Shanghai Jiao Tong University, Shanghai, China, and M.S. degree in Electrical and Computer Engineering from Georgia Institute of Technology, Atlanta, GA, USA, in 2011, 2014 and 2014 respectively. He's currently working toward the Ph.D. degree in Electrical and Computer Engineering at Georgia Institute of Technology.

His current research interests include vital sign detection, microwave Doppler radar, RF circuit design and phase locked loop.

Md. Mobashir Hasan Shandhi (S'17) received the BSc degree in Electrical and Electronics Engineering from Bangladesh University of Engineering & Technology (BUET), Dhaka, Bangladesh, in 2011 and the MSc degree in Electrical and Computer Engineering (ECE) from University of Utah, Salt Lake City, Utah, USA, in 2016. He is currently pursuing his Ph.D. degree in ECE at Georgia Institute of Technology, at Inan Research Lab under the supervision of Dr. Omer Inan.

He has worked as a lecturer in American International University - Bangladesh (AIUB), Dhaka, Bangladesh from 2011 to 2014. He has worked on MEMS arsenic sensor and high channel density neural array for large neuronal mapping. His current research includes wearable biomedical devices, home monitoring of cardiovascular health, signal processing algorithms and machine learning.

Omer T. Inan (S'06, M'09, SM'15) received the B.S., M.S., and Ph.D. degrees in electrical engineering from Stanford University, Stanford, CA, in 2004, 2005, and 2009, respectively.

He joined ALZA Corporation (A Johnson and Johnson Company) in 2006, where he designed micropower circuits for iontophoretic drug delivery. In 2007, he joined Countryman Associates, Inc., Menlo Park, CA where he was Chief Engineer, involved in designing and developing high-end professional audio circuits and systems. From 2009-2013, he was also a Visiting Scholar in the Department of Electrical Engineering, Stanford University. Since 2013, Dr. Inan is an Assistant Professor of Electrical and Computer Engineering at the Georgia Institute of Technology. He is also an Adjunct Assistant Professor in the Wallace H. Coulter Department of Biomedical Engineering. His research focuses on non-invasive physiologic sensing and modulation for human health and performance, including for chronic disease management, acute musculoskeletal injury recovery, and pediatric care.

Dr. Inan is an Associate Editor of the IEEE Journal of Biomedical and Health Informatics, Associate Editor for the IEEE Engineering in Medicine and Biology Conference and the IEEE Biomedical and Health Informatics Conference, Invited Member of the IEEE Technical Committee on Translational Engineering for Healthcare Innovation and the IEEE Technical Committee on Cardiopulmonary Systems, and Technical Program Committee Member or Track Chair for several other major international biomedical engineering conferences. He has published more than 125 technical articles in peer-reviewed international journals and conferences, and has six issued patents. Dr. Inan received the Gerald J. Lieberman Fellowship in 2009, the Lockheed Dean's Excellence in Teaching Award in 2016, the Sigma Xi Young Faculty Award in 2017, the Office of Naval Research Young Investigator Award in 2018, and the National Science Foundation CAREER Award in 2018. He was a National Collegiate Athletic Association (NCAA) All-American in the discus throw for three consecutive years (2001-2003).

Ying Zhang (M'07-SM'15) received a M.S. degree in materials engineering from the University of Illinois at Chicago, a M.S. degree in electrical engineering from the University of Massachusetts Lowell, and the Ph.D. degree in systems engineering from the University of California at Berkeley, in 2001, 2002, and 2006, respectively.

She is working as a Professor in the School of Electrical and Computer Engineering, Georgia Institute of Technology. Her research interests are in the areas of sensors and smart wireless sensing systems, power management for energy harvesting wireless sensor networks, intelligent monitoring and diagnostic systems, artificial intelligence, information retrieval and data mining, and computer aided optimal design.